Lawrence Berkeley National Laboratory

Title

Ultrafast dynamics of strong-field dissociative ionization of CH2Br2 probed by femtosecond soft x-ray transient absorption spectroscopy

Permalink

https://escholarship.org/uc/item/5tc0f7zm

Authors

Loh, Zhi-Heng
Leone, Stephen R.

Publication Date

2008-06-24

Peer reviewed

Ultrafast dynamics of strong-field dissociative ionization of CH_2Br_2 probed by femtosecond soft x-ray transient absorption spectroscopy

Zhi-Heng Loh and Stephen R. Leone[*]

Departments of Chemistry and Physics, University of California, Berkeley, CA 94720,

and Chemical Sciences Division, Lawrence Berkeley National Laboratory, 1 Cyclotron

Road, Berkeley, CA 94720

Abstract

Femtosecond time-resolved soft x-ray transient absorption spectroscopy based on a high-order harmonic generation source is used to investigate the dissociative ionization of CH_2Br_2 induced by 800 nm strong-field irradiation. At moderate peak intensities (2.0×10^{14} W/cm^2), strong-field ionization is accompanied by ultrafast C–Br bond dissociation, producing both neutral Br ($^2P_{3/2}$) and Br* ($^2P_{1/2}$) atoms together with the CH_2Br^+ fragment ion. The measured rise times for Br and Br* are 130 ± 22 fs and 74 ± 10 fs, respectively. The atomic bromine quantum state distribution shows that the Br/Br* population ratio is 8.1 ± 3.8 and that the Br $^2P_{3/2}$ state is not aligned. The observed product distribution and the timescales of the photofragment appearances suggest that multiple field-dressed potential energy surfaces are involved in the dissociative ionization process. In addition, the transient absorption spectrum of $CH_2Br_2^+$ suggests that the alignment of the molecule relative to the polarization axis of the strong-field ionizing pulse determines the electronic symmetry of the resulting ion; alignment of the Br—Br, H—H, and C_2 axis of the molecule along the polarization axis results in the production of the ion $\widetilde{X}\left(^2B_2\right)$, $\widetilde{B}\left(^2B_1\right)$ and $\widetilde{C}\left(^2A_1\right)$ states, respectively. At higher peak intensities (6.2×10^{14} W/cm^2), $CH_2Br_2^+$ undergoes sequential ionization to form the metastable $CH_2Br_2^{2+}$ dication. These results demonstrate the potential of core-level probing with high-order harmonic transient absorption spectroscopy for studying ultrafast molecular dynamics.

---

[*] Corresponding author. Electronic mail: srl@berkeley.edu

I. INTRODUCTION

In the interaction of an intense laser pulse with an atom, the electric field of the laser light ($\sim 1 \times 10^8$ V/cm) is comparable to the core potential experienced by the valence electron such that the ionization continuum threshold can be suppressed by the laser field.[1,2] The valence electron is then launched into the continuum by either tunnel ionization or strong-field multiphoton ionization.[3] Laser-dressing of the continuum results in above-threshold ionization,[4–6] whereby peaks spaced apart by the photon energy $\hbar\omega$ are present above the field-free binding energy in the photoelectron spectrum. Alternatively, recollision of the photoelectron with the ion core can lead to either radiative recombination or inelastic scattering and ejection of a second electron; the former results in high-order harmonic generation,[7–9] whereas the latter is the phenomenon of nonsequential double ionization.[10,11]

Analogous to the suppression of the core potential in strong-field laser-atom interaction, the irradiation of a molecule by an intense laser field results in distortions of the molecular potential energy surfaces. The nuclear degrees of freedom in the molecule therefore enable additional phenomena to be observed,[12,13] the most common of which is dissociative ionization.[14,15] Studies on the dissociative ionization of small molecules such as H_2 demonstrate effects such as bond softening,[16,17] above-threshold dissociation,[17,18] and vibrational trapping,[19,20] all of which can be rationalized within a field-dressed molecule framework. The dependence of the tunnel ionization rate on internuclear separation[21] enables the creation of a vibrational wavepacket in the electronic ground state of D_2 using few-cycle pulses.[22] With additional carrier-envelope phase stabilization, electron localization prior to the dissociative ionization of D_2 is observed.[23] For larger

2

molecules such as linear polyenes[24] and polycyclic aromatic hydrocarbons,[25] measuring

their extent of fragmentation as a function of laser peak intensity and wavelength reveal

the importance of nonadiabatic ionization and multielectron effects; these effects are

attributed to the presence of spatially delocalized, low-lying electronically excited states

in molecules with extensive π-conjugation. On the other hand, the atomic-like ionization

behavior of polyatomics such as alcohols[26] and methyl halides[27] can be attributed to the

localization on a single atom of the orbital that is ionized (typically the highest occupied

molecular orbital). In the extreme limit in which multiple electrons are removed via

strong-field ionization, the resultant highly charged species can undergo Coulomb

explosion.[28] Optical field-induced Coulomb explosion has found applications in the

reconstruction of dissociative wavepacket motion[29] and the direct imaging of rotational

alignment.[30] Finally, even in the absence of ionization, large ac Stark shifting of

molecular potentials induced by nonresonant strong-field laser pulses can be used to

control the branching ratio of chemical reactions.[31,32]

While many molecular strong-field ionization studies focus on measuring the yield

and kinetic energy release of the fragment ions as a function of laser peak intensity, the

recent application of femtosecond pump-probe techniques[33] enables the investigation of

molecular strong-field ionization from a time domain perspective. Time-resolved

measurements demonstrate the formation of an electronically excited I^{2+} fragment

produced by charge-asymmetric dissociation of I_2^{2+},[34] as well as the direct formation of

the I_2^{+} $A\left(^{2}\Pi_{u,3/2}\right)$ state by strong-field ionization of I_2 with 400 nm pulses.[35] Similar

studies performed on polyatomic species such as CH_2BrI show C–Br bond dissociation in

addition to the formation of a vibrational wavepacket along the CBrI bending coordinate;[36] in CH_2I_2, I_2^+ elimination is also observed after strong-field ionization.[37]

Here we employ a new method to study the strong-field dissociative ionization of a polyatomic molecule. Femtosecond time-resolved soft x-ray absorption spectroscopy is used to investigate the ultrafast dynamics of the molecular ions and atomic bromine fragments produced when CH_2Br_2 is subjected to strong-field ionization by an ultrashort pulse at 800 nm. Soft x-ray absorption allows direct spectroscopic probing of the various photofragment species through transitions originating from the Br $3d$ core level ($N_{4/5}$ edge). The soft x-ray light is generated by a table-top, laser-based setup using high-order harmonic generation, allowing the temporal evolution of the various neutral and ion photofragments produced by dissociative ionization to be measured with sub-50-fs time resolution. Recent work performed using this apparatus includes resolving the quantum state distribution of Xe^+ ions produced by optical strong-field ionization,[38] as well as observing the laser-dressing of He double excitation states.[39] This paper addresses the first soft x-ray core level study of its type on a molecular system, i.e., the dissociative and multiple ionization of CH_2Br_2. The experiments unveil numerous pathways that are involved in the interaction of an intense femtosecond pulse with a complex molecular system. The remainder of this paper is organized as follows. An overview of the experimental and computational methods employed in this study is given in Section II. Relevant results from previous spectroscopic studies of $CH_2Br_2^+$ are summarized in Section III. Results obtained at moderate and high laser peak intensities are presented in Sections IVA and IVB, respectively. The possibility of observing anisotropic molecular

strong-field ionization from the experimental results is discussed in Section IVC. Finally, this paper concludes with a summary of the key results in Section IV.

II. EXPERIMENTAL SETUP AND COMPUTATIONAL METHOD

The schematic of the experimental setup is illustrated in Fig. 1. The amplified output from a commercial Ti:sapphire laser system (2.5 W, 800 nm, 45 fs, 1 kHz) is sent to a 20:80 beamsplitter to produce the strong-field ionization and high-order harmonic generation beams, respectively. High-order harmonics in the soft x-ray region are generated by focusing the laser light into a 7 cm long, 150 μm internal diameter capillary filled with 8.0×10^3 Pa of Ne.[40] The estimated photon flux is 10^5 photons per pulse per harmonic. A pair of 0.2 μm thick Al foils is used to reject the residual 800 nm light and transmit the high-order harmonics. After reflection by a toroidal mirror, the high-order harmonics are refocused into a 2 mm long Teflon gas cell with 200 μm diameter entrance and exit pinholes. The pressure of the CH_2Br_2 sample gas target is 6.7×10^2 Pa. Gradual clogging of the gas cell entrance and exit pinholes due to laser-induced decomposition of CH_2Br_2 prevents higher sample densities from being used, at the expense of signal-to-noise. The transmitted soft x-ray radiation is spectrally dispersed in a home-built spectrometer and detected with a thermoelectrically cooled CCD camera. The accuracy of the spectrometer calibration is verified by using the $5p^{-1}\left(^2P_{3/2}\right) \rightarrow 4d^{-1}\left(^2D_{5/2}\right)$ transition of Xe^+ and the $^1S_0 \rightarrow 4d^{-1}\left(^2D_{5/2}\right)6p\left(^2P_{3/2}\right)$ transition of neutral Xe located at 55.4 eV and 65.1 eV, respectively.[41,42] Previous work on optical strong-field ionization of Xe gives an estimate of 30 fs FWHM for the soft x-ray pulse duration and a spectral resolution of 0.2 eV FWHM for the spectrometer.[38] Scanning knife-edge measurements

give a beam waist of 21 μm for the high-order harmonics at the interaction region. The weak continuum underlying the discrete harmonic peaks allows acquisition of the entire absorption spectrum without the need to tune the harmonic photon energies.

The 800 nm strong-field ionization beam is reflected by a pick-off mirror positioned 10 cm before the interaction region, which allows it to intersect with the soft x-ray probe beam at the sample gas cell with a 2$^{\text{o}}$ crossing angle. With a maximum available 800 nm pulse energy of 0.45 mJ incident on the gas cell and a focal beam waist of 32 μm, the maximum peak intensity of the strong-field ionization pulse is 6.2 $\times$ 10^{14} W/cm^2. For experiments at moderate peak intensities, an iris diaphragm inserted into the path of the pump beam is used to attenuate the pulse energy to 0.27 mJ; the resultant focal beam waist of 44 μm yields a peak intensity of 2.0 $\times$ 10^{14} W/cm^2. All measurements are performed with a parallel relative polarization between the pump and probe beams.

Transient absorption spectra are obtained by using high-order harmonic spectra collected at −500 fs time delay as the reference; a constant background offset due to stray pump beam light incident on the CCD camera precludes the use of the pump-off spectrum as the reference spectrum. A negative time delay implies that the probe pulse arrives at the sample before the pump pulse. The transient absorbance (optical density) is therefore defined as $\Delta OD(E, \Delta t) = -\log[I(E, \Delta t)/I(E, -500\text{fs})]$, where $I(E, \Delta t)$ is the spectral intensity of the soft x-ray light at photon energy E and time delay Δt. Transient absorption spectra are obtained from an average of 128 spectra, with the CCD integration time set to 2 s for each high-order harmonic spectra collected at positive and negative time delays. This procedure allows features with ΔOD as small as ~0.01 to be resolved in the transient absorption spectra. Pump-probe time traces are obtained by collecting the

high-order harmonic spectrum over a CCD integration time of 2 s at each time delay as the delay stage is scanned from –200 fs to 1000 fs (–250 fs to 1500 fs in the case of $CH_2Br_2^{2+}$); the ΔOD at each time delay is then computed by integrating the number of counts over a spectral bandwidth of 0.1 eV, and using the corresponding value obtained at negative time delays as reference. Eight sets of such time traces are then averaged to yield the time traces shown below. The delay stage is scanned in time steps of 20 fs for time delays between –200 fs and +200 fs, and in time steps of 50 fs for other time delays. Reported error bars correspond to 95% confidence interval limits.

The time trace for the rise of the $CH_2Br_2^{+}$ ground state absorption signal (Fig. 2a) mirrors the depletion of the neutral CH_2Br_2 absorption signal (Fig. 2b); both exhibit a characteristic field ionization response. These traces originate from the cross-correlation of the soft x-ray pulse duration with the increase in ionization yield within the 800 nm pulse envelope, which can be fit to a convolution of a step function with a Gaussian function. The FWHM values for the Gaussian function are 37 ± 12 and 37 ± 13 fs for the $CH_2Br_2^{+}$ and CH_2Br_2 signals, respectively. This FWHM value defines the instrumental time resolution and is incorporated as an instrument response function in the fitting routine for the collected time traces. The time constants reported below are obtained after deconvolving the instrument response from the time traces. From the depletion of the neutral CH_2Br_2 signal ($\Delta OD = -0.03$) and the static absorbance of the sample (OD = 0.066), it is estimated that ~50% of the CH_2Br_2 sample in the probe volume is ionized.

Density functional theory calculations for $CH_2Br_2^{2+}$ and CH_2Br^{+} are carried out using the GAUSSIAN 98 program package.[43] Gradient corrections to the local density approximation are introduced in a self-consistent manner using the three-parameter

Becke (B3) hybrid exchange functional[44] and the correlation functional of Lee, Yang, and Parr (LYP).[45] The triple-zeta basis set 6-311G(d,p) is employed. Vibrational frequency calculations are carried out on optimized ground and transition state structures to ensure that they correspond to a local minimum and a first-order saddle point, respectively; in the case of the transition state, it is further verified that the imaginary frequency arises from the C–Br asymmetric stretching mode, which is the active mode in the dissociation process. Reported energy values include corrections for zero point vibrational energies. The computed vibrational frequencies are in good agreement with experimental values, thus verifying the accuracy of the calculation results.

III. PREVIOUS SPECTROSCOPIC STUDIES OF THE $CH_2Br_2^+$ ION

Photoionization of CH_2Br_2 in a frozen Ar matrix enables the isolation and subsequent spectroscopic characterization of $CH_2Br_2^+$.[46] The optical absorption spectrum of $CH_2Br_2^+$ has a prominent absorption peak at 3.42 eV that is assigned to the $\widetilde{D}\left(^2B_2\right)\leftarrow\widetilde{X}\left(^2B_2\right)$ transition. (To avoid ambiguity when consulting the character table for the C_{2v} point group, we note here that the CBr_2 moiety lies in the $\sigma_v(yz)$ plane.) This assignment is substantiated by the photoelectron spectrum of CH_2Br_2, which gives a vertical ionization potential of 10.61 eV and the location of the ion $\widetilde{D}$ state at 14.12 eV above the neutral ground state.[47] The slight deviation of the corresponding $\widetilde{D}-\widetilde{X}$ energy gap of 3.51 eV from the position of the near-UV absorption peak can be attributed to a difference in the Franck-Condon factors for the two photoionization transitions and the transition for the ion.

The absence of vibrational structure in the photoelectron band at 14.12 eV suggests that the ion $\widetilde{D}$ state undergoes rapid dissociation.[47] This is verified by a photofragment ion imaging study, in which simultaneous irradiation of CH_2Br_2 with both the 9th and the 3rd harmonic of a nanosecond Nd:YAG laser (10.49 eV and 3.50 eV, respectively) results in the photodissociation of $CH_2Br_2^+$.[48] A power dependence measurement confirms that the 9th harmonic ionizes the neutral molecule to form the ion ground state via a single-photon process, and the 3rd harmonic excites the ion ground state to the dissociative ion $\widetilde{D}$ state. Note that the ion $\widetilde{D}$ state is the lowest ion excited state that is energetically allowed to dissociate to give Br*; this state is located 14.12 eV above the neutral ground state,[47] whereas the adiabatic appearance energy of CH_2Br^+ + Br* is 11.68 eV.[49] The CH_2Br^+ photofragment translational energy distribution suggests that photodissociation from the ion $\widetilde{D}$ state gives both Br and Br* (spin-orbit-excited Br atom) in the ratio Br/Br* = 0.45. An energy level diagram that correlates the various dissociation products to the initial $CH_2Br_2^+$ ion state is shown in Fig. 3; this diagram is constructed with the aid of symmetry arguments previously applied to the study of CH_2I_2 photodissociation.[50–53] From the energy level diagram, it is seen that the ion $\widetilde{D}$ state correlates adiabatically to CH_2Br^+ + Br*; the formation of Br atoms observed in the photofragment ion imaging study could originate from a symmetry-allowed nonadiabatic curve crossing[54,55] involving the ion $\widetilde{C}\left(^2A_1\right)$ state.

IV. RESULTS AND DISCUSSION

The goal of this work is to elucidate the various processes and their associated time scales that are encountered in the interaction of CH_2Br_2 with a strong laser field. Towards

this end, experiments are carried out at two peak intensities of the strong-field ionization pulse – the first set of experiments is performed at a moderate peak intensity (electric field strength) of 2.0×10^{14} W/cm^2 (3.9×10^8 V/cm) and the second set of experiments is performed at a higher peak intensity (electric field strength) of 6.2×10^{14} W/cm^2 (6.8×10^8 V/cm). In both sets of experiments, soft x-ray transient absorption spectra are collected to identify the various species produced by strong-field ionization, and time-resolved measurements are performed to measure the timescales accompanying the formation of the various photoproducts. At the high field strengths employed in this work, the known states of the parent ion can be dressed by the laser field, resulting in product distributions and dynamics that are different compared to those obtained from the photofragment ion imaging study[48] noted above.

A. C–Br BOND DISSOCIATION AT MODERATE PEAK INTENSITY

The soft x-ray transient absorption spectrum collected at a time delay of 500 fs and a moderate peak intensity of 2.0×10^{14} W/cm^2 for the strong-field ionization pulse is shown in Fig. 4. The transient absorption peaks at 64.4 eV, 65.1 eV, and 65.4 eV correspond to the Br atom $^2P_{3/2} \rightarrow {}^2D_{5/2}$, $^2P_{1/2} \rightarrow {}^2D_{3/2}$, and $^2P_{3/2} \rightarrow {}^2D_{3/2}$ transitions, respectively.[56] The observation of both Br and Br* spin-orbit components suggests that multiple potential energy surfaces are involved in the dissociation process. The relative peak areas of the three transitions can be used to extract the spin-orbit and alignment distribution of the Br atoms. By defining the quantization axis to be parallel to the soft x-ray probe polarization axis, the peak areas of the various transitions (apart from a constant factor) are given by

10

$$A\left({}^2P_{3/2} \rightarrow {}^2D_{5/2}\right) = \left(\frac{1}{10}\rho_{3/2,1/2} + \frac{1}{15}\rho_{3/2,3/2}\right)\left|\left\langle 3d_{5/2}^{-1}\|d\|4p_{3/2}^{-1}\right\rangle\right|^2,\tag{1a}$$

$$A\left({}^2P_{1/2} \rightarrow {}^2D_{3/2}\right) = \frac{1}{6}\rho_{1/2,1/2}\left|\left\langle 3d_{3/2}^{-1}\|d\|4p_{1/2}^{-1}\right\rangle\right|^2,\ \text{and}\tag{1b}$$

$$A\left({}^2P_{3/2} \rightarrow {}^2D_{3/2}\right) = \left(\frac{1}{60}\rho_{3/2,1/2} + \frac{3}{20}\rho_{3/2,3/2}\right)\left|\left\langle 3d_{3/2}^{-1}\|d\|4p_{3/2}^{-1}\right\rangle\right|^2,\tag{1c}$$

where $\rho_{j,|m|} = \rho_{j,+m} + \rho_{j,-m}$ denotes the total probability of producing the Br atom in the quantum state with total angular momentum j and projection quantum number of $+m$ and $-m$, $\left\langle q\|d\|p\right\rangle$ is the reduced transition dipole matrix element for the $p \rightarrow q$ transition, and d is the electric dipole operator. The reduced transition dipole matrix elements are obtained from a multiconfiguration Dirac-Fock calculation performed with the program package GRASP2,[57] which yields $\left|\left\langle 3d_{5/2}^{-1}\|d\|4p_{3/2}^{-1}\right\rangle\right|^2 : \left|\left\langle 3d_{3/2}^{-1}\|d\|4p_{1/2}^{-1}\right\rangle\right|^2 : \left|\left\langle 3d_{3/2}^{-1}\|d\|4p_{3/2}^{-1}\right\rangle\right|^2$ = 0.14 : 0.082 : 0.015. The measured quantum state distribution is then $\rho_{3/2,1/2} : \rho_{3/2,3/2} : \rho_{1/2,1/2}$ = 46 ± 12 : 43 ± 14 : 11 ± 2%, corresponding to a Br/Br* branching ratio of 8.1 ± 3.8. The absence of orbital alignment in the Br $^2P_{3/2}$ state is unsurprising, given the thermal ensemble of rotational states present in the CH_2Br_2 sample; this is in contrast with the hole orbital alignment previously observed in the cylindrically symmetric problem of atomic strong-field ionization of Kr and Xe with linearly polarized light.[38,58] Moreover, dissociation along multiple potential energy surfaces, a scenario frequently encountered in strong-field dissociative ionization of molecules,[12,13] can also lead to the loss of photofragment orbital alignment.[59]

In addition to the neutral Br and Br* peaks, absorption features due to the $CH_2Br_2^+$ parent ion and the CH_2Br^+ dissociative ionization fragment ion are also observed in the transient absorption spectrum. The parent ion ground state signal is at 66.5 eV, whereas

the fragment ion ground state absorption peak is located at 67.3 eV. Within a single-particle picture,[60,61] the probe transitions in these ground state molecular ions involve the promotion of a Br $3d$ core electron to the singly occupied molecular orbital of the parent ion ($CH_2Br_2^+$) or the lowest unoccupied molecular orbital of the fragment ion (CH_2Br^+). The energies of the core-to-valence transitions can therefore be estimated from the Br $3d$ core level binding energies and the vertical ionization potentials of the corresponding neutral species. In the absence of an available value for the Br $3d$ core level binding energy for CH_2Br_2 and CH_2Br, the value of 76.24 eV for CH_3Br is used instead.[62] The vertical ionization potentials of CH_2Br_2 and CH_2Br are 10.61 eV and 8.72 eV, respectively.[47,63] These values give 65.63 eV and 67.52 eV for the core-to-valence transition energies of $CH_2Br_2^+$ and CH_2Br^+ in their ground states, respectively, which are in modest agreement with the energies of the assignments. It is important to note that, since vertical ionization potentials are used in the above calculation, the estimated transition energies correspond to those in the Franck-Condon window of the neutral species at its equilibrium geometry. Since the transient absorption spectrum is acquired at a time delay of 500 fs, the relevant Franck-Condon window differs from that mentioned above. Nevertheless, the measured temporal responses provide further strong support for the peak assignments, as the peak that is assigned to the $CH_2Br_2^+$ parent ion yields a time trace that is indicative of the prompt field ionization response (Fig. 2a), whereas the time trace for the peak that is assigned to the CH_2Br^+ fragment ion is suggestive of the much slower dissociation process as its origin (see below).

The shoulder observed to the low energy side (66.0 eV) of the $CH_2Br_2^+$ ground state ion absorption suggests that strong-field ionization of CH_2Br_2 also yields excited states of

the parent ion in addition to the ground state. The energy shift of 0.50 eV is in relatively good agreement with the vertical $\widetilde{B}\left({}^2B_1\right) \leftarrow \widetilde{X}\left({}^2B_2\right)$ and $\widetilde{C}\left({}^2A_1\right) \leftarrow \widetilde{X}\left({}^2B_2\right)$ transition energies of 0.67 eV for the ion estimated from the photoelectron spectrum of CH_2Br_2;[47] the slight deviation could be due to the fact that the 45 fs pulse used for strong-field ionization allows the molecule sufficient time to move away from the vibrational Franck-Condon region before it is completely ionized, i.e., strong-field ionization is not a strictly vertical transition. In addition to the $\widetilde{B}$ and/or $\widetilde{C}$ states of the ion, population of the ion $\widetilde{A}\left({}^2A_2\right)$ state is also possible, although the energy shift of 0.2 eV from the $\widetilde{X}$ state is too small to be spectrally resolved.[47] The observation of population in the ion $\widetilde{B}$ and/or $\widetilde{C}$ state suggests that it is important to analyze molecular strong-field ionization phenomena beyond the framework established by the tunnel ionization model,[64–66] since such a model does not account for the existence of molecular excited states that could play an important role in the ionization process.

The time traces for the appearance of the Br and Br* absorption signals are obtained by monitoring the peaks of the ${}^2P_{3/2} \rightarrow {}^2D_{5/2}$ and ${}^2P_{1/2} \rightarrow {}^2D_{3/2}$ transitions, respectively (Fig. 5a). The measured Br and Br* rise times are 130 ± 22 fs and 74 ± 10 fs, respectively. Surprisingly, the ground state atom rises more slowly than the spin-orbit excited state atom, indicating more complex dynamics than the production of the two atomic states from a single dissociative ion state. The most plausible explanation for the different rise times of Br and Br* is that strong-field ionization populates multiple dissociative or predissociative ionic states in the Franck-Condon region that correlate to different fine structure states for the Br atom product. Alternatively, dissociation can originate from the ion $\widetilde{D}\left({}^2B_2\right)$ state, which has been shown to dissociate to give a

13

mixture of Br and Br* via a nonadiabatic curve crossing.[48] In this case, the different time constants measured for the Br and Br* channels could originate from a probe window effect,[67,68] in which the dissociative wavepackets approach with different terminal velocities or at different times the region of the potential energy surface in which the free atomic bromine core-level transition is resonant with the soft x-ray probe photon energy. A probe window effect has been used to explain the different appearance times for atomic I and I* in the UV photoinduced dissociation of ICN and CH_3I.[69,70] Dissociation in the Rydberg manifold can also occur, in principle, via multiphoton excitation of the neutral ground state. Due to the low ionization potentials of neutral Rydberg states, however, these states are expected to undergo ionization before significant dissociation can occur within the temporal envelope of the laser pulse.[15] Moreover, the time trace for the CH_2Br^+ fragment ion (Fig. 5b) can also be fit to a biexponential rise with time constants of 130 fs and 74 fs in an $8.5 \pm 1.7 : 1$ amplitude ratio (Br/Br*), in good agreement with the measured ratio from the atomic Br signals (8.1 ± 3.8). The concomitant formation of CH_2Br^+ with Br and Br* suggests that dissociation does occur on the $CH_2Br_2^+$ potential energy surfaces. The poor signal-to-noise ratio of the time traces prevents a complete set of free-floating parameters from being used in the biexponential fitting routine; instead, the time constants are fixed to those measured for the Br and Br* signals, while their relative amplitudes are allowed to vary. Finally, contamination of the observed temporal dynamics from sequential ionization of Br to Br^+ within the temporal envelope of the 800 nm pulse can be excluded on the basis of time-of-flight mass spectra collected on another apparatus under similar strong-field ionization conditions (800 nm peak intensity of $2.1 \times$

10^{14} W/cm^2). These spectra exhibit a relative CH_2Br^+/Br^+ peak area ratio of >30:1; this amount of Br^+ is below the detection limit of our apparatus ($\Delta OD \sim 0.01$).

In the absence of accurate potential energy surfaces for the excited states of $CH_2Br_2^+$, it is not possible to identify the precise dissociation pathway(s) that dominate. Nevertheless, the presence of the strong laser field during early times of the C–Br bond dissociative ionization process requires the consideration of multiple field-dressed potential energy surfaces in explaining the observed product branching ratio and dynamics. One example to consider is the dramatic difference of the Br/Br* branching ratio measured in this work from that reported in the photofragment ion imaging study,[48] in which weak-field excitation was employed. In addition, the reported anisotropy parameters β in the weak-field excitation case for the Br ($\beta = 1.8$) and Br* ($\beta = 1.5$) channels suggest that dissociation in the former channel is more rapid;[48] by treating Br–CH$_2$Br as a pseudodiatomic in which each fragment is reduced to a point mass, dissociation lifetimes of 121 fs and 240 fs might be inferred from the β values for the Br and Br* channels,[71,72] respectively. These lifetimes are considerably different, as well as reversed in order, from the rise times for Br and Br* reported herein.

The dissociation time scales and branching ratios reported in the present work will provide a starting point for further experimental work using femtosecond transition state spectroscopy[73,74] with shorter soft x-ray probe pulses, as well as to complement future theoretical exploration of strong-field dissociative ionization employing wavepacket propagation techniques.[75,76] These studies will enable the reconstruction of the dissociative wavepacket trajectory along different parts of the field-dressed potential energy surfaces.

B. CH$_2$Br$_2^{2+}$ DICATION FORMATION AT HIGHER PEAK INTENSITY

The transient absorption spectrum collected at a time delay of 500 fs and a high peak intensity of 6.2×10^{14} W/cm^2 for the 800 nm pulse is shown in Fig. 6a. At this peak intensity, separate measurements on the strong-field ionization of Xe show that production of the Xe^{2+} dominates over that of Xe$^+$. In contrast to the transient absorption spectrum collected at a lower peak intensity of the 800 nm pulse, this spectrum does not exhibit any absorption peaks in the neutral atomic Br region (Fig. 6a inset). The absorption peak at 67.3 eV for the CH$_2$Br$^+$ photofragment is likewise absent. The peaks at 66.5 eV and 67.5 eV are assigned to the CH$_2$Br$_2^+$ ion, whereas the peaks at 68.9 eV and 69.9 eV are assigned to the CH$_2$Br$_2^{2+}$ dication. The depletion signal of the neutral CH$_2$Br$_2$ molecule appears at 70.5 eV and 71.6 eV in the transient absorption spectrum. The energy separation between the pair of peaks for all of the above molecular species are ~1 eV, which reflects the spin-orbit splitting of 1.05 eV for the Br $3d$ core level.[56]

It is important to note that the absences of absorption signals from the neutral atomic Br and the CH$_2$Br$^+$ dissociative ionization fragment does not necessarily imply the absence of C–Br bond dissociation, since elimination of Br$^+$, Br$_2^+$, Br$_2$, HBr$^+$ and HBr could also occur. In fact, recent results on the strong-field ionization of CH$_2$I$_2$ showed that I$_2^+$ elimination from CH$_2$I$_2^+$ also occurs via excitation of the CI$_2$ bending mode vibration.[37] However, I$_2^+$ elimination remains a minor channel (~10%) compared to C–I bond dissociation to give CH$_2$I$^+$ and I. Similarly, in the case of CH$_2$Br$_2^+$, atomic Br formation due to C–Br bond dissociation is expected to dominate over Br$_2^+$ elimination. The complete absence of the Br atom product therefore makes it unlikely that the pair of

peaks at 68.9 eV and 69.9 eV, which are assigned to the $CH_2Br_2^{2+}$ dication, is due to Br_2^+

formation. The elimination of Br^+, Br_2, HBr, and HBr^+ with significant yields can all be

excluded due to the absence of their spectral signatures in the transient absorption

spectrum.[56,62]

The absence of C–Br bond dissociation to form neutral atomic Br at high peak

intensity is in stark contrast to the dissociative ionization that occurs at moderate peak

intensity. This observation can be explained by the sequential ionization of $CH_2Br_2^+$ to

yield $CH_2Br_2^{2+}$ before the monocation has sufficient time to dissociate, which is

analogous to the argument put forth to exclude formation of Br and Br* via neutral

Rydberg channels (see above). However, upon formation of the dication, Coulomb

explosion might be expected to occur within 100 fs. Assuming a purely Coulombic

repulsive potential and treating Br^+–CH_2Br^+ as a pseudodiatomic, the C–Br bond length

of the dication would elongate by a factor of two in ~80 fs. The observation of $CH_2Br_2^{2+}$

in the transient absorption spectrum is therefore intriguing, since it indicates that the

lifetime of the dication is prolonged by a barrier to dissociation. The pump-probe time

trace, obtained by monitoring the $CH_2Br_2^{2+}$ absorption signal at 68.9 eV, further confirms

the significant stability of the dication up to a time delay of 1.5 ps (Fig. 6b).

Electronic structure calculations employing density functional theory were performed

to rationalize the stability of the dication. The energy level diagram calculated at the

B3LYP/6-311G(d,p) level of theory is shown in Fig. 7. The optimized geometric

parameters for the $CH_2Br_2^{2+}$ ground and transition states, as well as those for the CH_2Br^+

ground state are summarized in Table I. The calculations reveal that the Coulomb

explosion of $CH_2Br_2^{2+}$ to form CH_2Br^+ and Br^+ is thermodynamically favored. However,

17

a transition state exists along the Br^+–CH_2Br^+ dissociation coordinate and is located 1.94 eV above the $CH_2Br_2^{2+}$ ground state in its equilibrium geometry. In addition, RRKM calculations[77] show that an excess energy of 0.7 eV above this barrier is required for the dissociation rate to be 1×10^{11} s^{-1}, corresponding to a lifetime of 10 ps (cf. the dication is observed to be significantly stable up to 1.5 ps). From the Franck-Condon region (assuming a vertical double ionization transition from the CH_2Br_2 equilibrium geometry), however, the dication would possess 0.67 eV of internal energy. This amount of internal energy is insufficient to overcome the activation barrier. The $CH_2Br_2^{2+}$ dication observed in this work therefore joins a host of many other polyatomic dications that are metastable.[78]

C. ANISOTROPY OF MOLECULAR STRONG-FIELD IONIZATION

Measurements on rotationally aligned samples of linear molecules reveal a dependence of the ionization probability on the relative angle between the molecular axis and the polarization axis of the strong-field ionizing pulse.[79–81] This angular dependence can be explained in terms of the interference between the outgoing photoelectron partial waves that originate from different atomic sites of the molecule, thereby reflecting the symmetry of the orbital from which the electron is ejected.[82,83] In this section, a consideration of the anisotropic strong-field ionization of CH_2Br_2 provided by the experimental data is discussed. We consider only the transient absorption spectrum shown in Fig. 4, which is collected at a moderate peak intensity (2.0×10^{14} W/cm^2) of the 800 nm strong-field ionizing pulse.

First, we begin with a brief summary of the effect of ligand-field splitting on core-hole energy levels. As a result of spin-orbit coupling, the $3d$ core-hole levels of atomic Br are split into $3d_{5/2}$ $\left(^2D_{5/2}\right)$ and $3d_{3/2}$ $\left(^2D_{3/2}\right)$ states. When incorporated into a molecular framework, ligand-field splitting breaks the degeneracy of these states,[84,85] akin to the ligand-field splitting of transition metal d-orbitals in inorganic coordination chemistry. For molecules in which the bromine atom possesses local $C_{\infty v}$ symmetry, the $3d_{5/2}$ state splits into $^2\Sigma_{1/2}^+$, $^2\Pi_{3/2}$, and $^2\Delta_{5/2}$ states, whereas the $3d_{3/2}$ state splits into $^2\Pi_{1/2}$ and $^2\Delta_{3/2}$ states (Fig. 8). However, ligand-field splitting of the Br $3d$ core levels ($\sim0.1 - 0.2$ eV) is small compared to the Br $3d$ spin-orbit splitting (~1 eV). The coarse-scale structure of the Br $3d$ photoelectron and photoabsorption spectra is therefore dominated by two main peaks spaced ~1 eV apart (commonly attributed to the $3d_{5/2}$ and $3d_{3/2}$ core hole states), as confirmed by experiment.[62]

From the above discussion, it might seem surprising that the $CH_2Br_2^+$ and CH_2Br^+ absorption features in Fig. 4 are both present only as single peaks. This observation suggests that the probe transition leaves the Br $3d$ core level (almost) exclusively in the $^2\Sigma_{1/2}^+$ final state, since probing to either the Π and/or Δ state would manifest itself in the appearance of both $3d_{5/2}$ and $3d_{3/2}$ peaks. For the $CH_2Br_2^+$ ion ground state, for example, the $3d_{3/2}$ peak should appear at 67.5 eV. It is possible that this peak is masked by the CH_2Br^+ ground state absorption peak at 67.3 eV. However, the transient absorption spectrum in the 67.3 eV spectral region can be adequately fit to a single peak (that of the CH_2Br^+ ground state), which suggests that the $3d_{3/2}$ component of $CH_2Br_2^+$ ground state absorption, if present, is below the detection limit of our apparatus. The undetected $3d_{3/2}$

component therefore lends support to the assignment that the probe transition selectively accesses the $^2\Sigma_{1/2}^+$ final core hole state (Fig. 8).

From a group theoretical consideration, the probe transition is symmetry-allowed only when

$$\Gamma_i \otimes \Gamma_{pol} \otimes \Gamma_f \supseteq A_1, \qquad (2)$$

where Γ_i and Γ_f are the irreducible representations of the initial and final state symmetries, respectively, and Γ_{pol} is the irreducible representation for the probe polarization. Furthermore,

$$\Gamma_f = \Gamma_{f,c} \otimes \Gamma_{f,v}, \qquad (3)$$

where $\Gamma_{f,c}$ and $\Gamma_{f,v}$ are the irreducible representations for the core hole and valence orbital configurations of the final state that are involved in the probe transition. For the $CH_2Br_2^+$ ion ground state, the probe transition corresponds to the promotion of a Br $3d$ electron to the singly occupied b_2 valence orbital, resulting in a completely filled valence shell. Hence, $\Gamma_i = b_2$ and $\Gamma_{f,v} = a_1$. For the core hole state to belong to the totally symmetric irreducible representation (note that Σ^+ in $C_{\infty v}$ symmetry correlates to A_1 in C_{2v} symmetry), the probe polarization axis must belong to the b_2 irreducible representation. Since the relative polarization between the pump and probe pulses is parallel, this result suggests that in the thermal ensemble of CH_2Br_2 molecules, the sub-ensemble with their Br—Br axis aligned parallel to the polarization axis of the pump beam is preferentially ionized to form the $CH_2Br_2^+$ ion ground state. Applying a similar argument to the $CH_2Br_2^+$ $\tilde{B}(^2B_1)$ and $\tilde{C}(^2A_1)$ states suggests that these ion states are created by preferential ionization of the sub-ensemble of molecules with their H—H and C_2 axes aligned along the polarization axis of the pump pulse, respectively. We therefore arrive at

the empirical observation that the symmetry of the ion state that is preferentially produced by strong-field ionization is the same as the irreducible representation of the polarization axis of the strong-field ionizing pulse, i.e., $\Gamma_i = \Gamma_{pol}$.

Experimental and theoretical studies to date on the anisotropy of molecular strong-field ionization have focused on molecules with inversion symmetry,[79–83] thus preventing a direct comparison to be made between the results in the literature and those obtained in this study. However, we note that the b_1 orbital of CH_2Br_2, when viewed along the Br—Br axis, resembles the HOMO of ethylene (C_2H_4); *ab initio* calculations on C_2H_4 employing the Keldysh-Faisal-Reiss model predict that ionization is strongly enhanced along the axis orthogonal to the molecular plane.[86] This result agrees with our hypothesis that the $CH_2Br_2^+$ $\tilde{B}\left(^2B_1\right)$ state is formed from preferential ionization of the sub-ensemble of molecules with its H—H axis aligned parallel to the polarization axis of the pump pulse.

For the CH_2Br^+ ion ground state, the probe transition corresponds to the promotion of a Br $3d$ electron to the lowest unoccupied molecular orbital of b_2 symmetry. Hence, $\Gamma_i = a_1$ and $\Gamma_{f,v} = b_2$. Exclusive population of the $^2\Sigma_{1/2}^+$ core hole state by the soft x-ray probe, as suggested by the presence of a single peak in its transient absorption spectrum, requires the probe polarization axis to be orthogonal to the plane of the molecule. However, dissociation of the C–Br bond in $CH_2Br_2^+$, with its bent Br–CH_2–Br geometry in the Franck-Condon region, is expected to be accompanied by significant rotational excitation of the CH_2Br^+ fragment,[87,88] resulting in an ensemble of CH_2Br^+ ions with a spread in relative angles between the C–Br bond axis and the polarization axis of the soft

x-ray probe. Hence it is surprising that only a single absorption peak is observed for CH_2Br^+ instead of the spin-orbit doublet. This discrepancy warrants further investigation.

Finally, the degree of anisotropy for the strong-field ionization of CH_2Br_2 can be estimated as follows. For the $CH_2Br_2^+$ ion ground state, we argued above that a probe transition dipole along the Br—Br axis accesses the final core hole state with a totally symmetric representation, resulting in only the $3d_{5/2}$ peak being observed in the transient absorption spectrum. For the $3d_{3/2}$ peak to be observed as well, the transition dipole for the corresponding transition must be orthogonal to the Br—Br axis, i.e., along either the H—H axis or the C_2 axis. Given the detection limit of ΔOD ~ 0.01 and the maximum ΔOD of 0.08 for the $CH_2Br_2^+$ ground state absorption signal, the absorption signal for the probe transitions along the H—H and C_2 axes must be at least 8 times less than the absorption signal for the probe transition along the Br—Br axis. Taking into consideration that the signal intensity for a one-photon probe transition is proportional to $\cos^2\theta$, where θ is the relative angle between the transition dipole moment and the polarization axis of the probe pulse, we can infer that ionization to give the ion ground state occurs when the polarization axis of the strong-field ionizing pulse is within an estimated angular range of 15° about the Br—Br axis. That is, only the sub-ensemble of molecules in the isotropic sample with its Br—Br axis aligned within 15° of the polarization axis of the pump pulse is ionized to form the ion ground state; this degree of anisotropy is comparable to that reported recently for the strong-field ionization of CO_2.[81] Applying a similar logic to the $CH_2Br_2^+$ $\widetilde{B}$ and $\widetilde{C}$ states suggests that these states are created when ionization is confined to an estimated angular range of 35° about the H—H axis and C_2 axis, respectively. We emphasize that the observations and analysis presented

in this section are preliminary. However, a systematic study that involves varying the relative angle between the strong-field ionizing pump pulse and the soft x-ray probe pulse should enable retrieval of the complete angular dependence of the ionization yield for the various ion states.

V. CONCLUSIONS

Studies of molecular strong-field dissociative ionization reported to date have focused on measuring the photofragment yield as a function of laser peak intensity. In this work, we employ femtosecond time-resolved soft x-ray transient absorption spectroscopy to investigate strong-field dissociative ionization of CH_2Br_2 in the time domain. The soft x-ray light is produced on a table-top, laser-based setup via high-order harmonic generation. At a moderate 800 nm peak intensity of 2.0×10^{14} W/cm^2, C–Br bond dissociation is observed with counterintuitive Br and Br* rise times of 130 ± 22 fs and 74 ± 10 fs, respectively. The atomic bromine quantum state distribution shows that the Br/Br* population ratio is 8.1 ± 3.8 and that the Br $^2P_{3/2}$ state is not aligned. Since the strong laser field is still present during the early part of the C–Br bond dissociative ionization, it is necessary to interpret these results in terms of dynamics occurring on multiple field-dressed potential energy surfaces. In addition, the transient absorption spectrum suggests that the symmetry of the ion state that is preferentially produced is the same as the irreducible representation of the polarization axis along which strong-field ionization occurs, resulting in the creation of a molecular ion sample in which the ion states are aligned along a particular axis. At a high 800 nm peak intensity of 6.2×10^{14} W/cm^2, sequential ionization of $CH_2Br_2^+$ to $CH_2Br_2^{2+}$ is observed. Experimental data

shows that the dication species is metastable with respect to Coulomb explosion, in agreement with results obtained from electronic structure calculations. This study demonstrates the utility of femtosecond high-order harmonic transient absorption spectroscopy for core-level probing of ultrafast molecular dynamics. Studies are currently being performed on the isomerization dynamics of transient carbocations generated by strong-field dissociative ionization.

REFERENCES

1. T. Brabec and F. Krausz, Rev. Mod. Phys. **72**, 545 (2000).

2. M. Protopapas, C. H. Keitel, and P. L. Knight, Rep. Prog. Phys. **60**, 389 (1997).

3. P. B. Corkum, Phys. Rev. Lett. **71**, 1994 (1993).

4. P. Agostini, F. Fabre, G. Mainfray, G. Petite, and N. K. Rahman, Phys. Rev. Lett. **42**, 1127 (1979).

5. P. B. Corkum, N. H. Burnett, and F. Brunel, Phys. Rev. Lett. **62**, 1259 (1989).

6. R. R. Freeman, P. H. Bucksbaum, H. Milchberg, S. Darack, D. Schumacher, and M. E. Geusic, Phys. Rev. Lett. **59**, 1092 (1987).

7. A. McPherson, G. Gibson, H. Jara, U. Johann, T. S. Luk, I. A. McIntyre, K. Boyer, and C. K. Rhodes, J. Opt. Soc. Am. B **4**, 595 (1987).

8. A. L'Huillier and Ph. Balcou, Phys. Rev. Lett. **70**, 774 (1993).

9. J. J. Macklin, J. D. Kmetec, and C. L. Gordon, III, Phys. Rev. Lett. **70**, 766 (1993).

10. B. Walker, B. Sheehy, L. F. DiMauro, P. Agostini, K. J. Schafer, and K. C. Kulander, Phys. Rev. Lett. **73**, 1227 (1994).

11. D. N. Fittinghoff, P. R. Bolton, B. Chang, and K. C. Kulander, Phys. Rev. Lett. **69**, 2642 (1992).

12. A. Giusti-Suzor, F. H. Mies, L. F. DiMauro, E. Charron, and B. Yang, J. Phys. B **28**, 309 (1995).

13. J. H. Posthumus, Rep. Prog. Phys. **67**, 623 (2004).

14. K. Codling and L. J. Frasinski, J. Phys. B **26**, 783 (1993).

15. R. J. Levis and M. J. DeWitt, J. Phys. Chem. A **103**, 6493 (1999).

16. P. H. Bucksbaum, A. Zavriyev, H. G. Muller, and D. W. Schumacher, Phys. Rev. Lett. **64**, 1883 (1990).

17. A. Zavriyev, P. H. Bucksbaum, J. Squier, and F. Saline, Phys. Rev. Lett. **70**, 1077 (1993).

18. A. Giusti-Suzor, X. He, O. Atabek, and F. H. Mies, Phys. Rev. Lett. **64**, 515 (1990).

19. A. Giusti-Suzor and F. H. Mies, Phys. Rev. Lett. **68**, 3869 (1992).

20. G. Yao and S.-I. Chu, Chem. Phys. Lett. **197**, 413 (1992).

21. X. Urbain, B. Fabre, E. M. Staicu-Casagrande, N. de Ruette, V. M. Andrianarijaona, J. Jureta, J. H. Posthumus, A. Saenz, E. Baldit, and C. Cornaggia, Phys. Rev. Lett. **92**, 163004 (2004).

22. Th. Ergler, B. Feuerstein, A. Rudenko, K. Zrost, C. D. Schröter, R. Moshammer, and J. Ullrich, Phys. Rev. Lett. **97**, 103004 (2006).

23. M. F. Kling, Ch. Siedschlag, A. J. Verhoef, J. I. Khan, M. Schultze, Th. Uphues, Y. Ni, M. Uiberacker, M. Drescher, F. Krausz, and M. J. J. Vrakking, Science **312**, 246 (2006).

24. M. Lezius, V. Blanchet, D. M. Rayner, D. M. Villeneuve, A. Stolow, and M. Yu. Ivanov, Phys. Rev. Lett. **86**, 51 (2001); M. Lezius, V. Blanchet, M. Yu. Ivanov, and A. Stolow, J. Chem. Phys. **117**, 1575 (2002).

25. A. N. Markevitch, S. M. Smith, D. A. Romanov, H. B. Schlegel, M. Yu. Ivanov, and R. J. Levis, Phys. Rev. A **68**, 011402 (2003).

26. D. Mathur, T. Hatamoto, M. Okunishi, G. Prümper, T. Lischke, K. Shimada, and K. Ueda, J. Phys. Chem. A **111**, 9299 (2007).

27. M. Tanaka, M. Murakami, T. Yatsuhashi, and N. Nakashima, J. Chem. Phys. **127**, 104314 (2007).

28. D. T. Strickland, Y. Beaudoin, P. Dietrich, and P. B. Corkum, Phys. Rev. Lett. **68**, 2755 (1992).

29. H. Stapelfeldt, E. Constant, and P. B. Corkum, Phys. Rev. Lett. **74**, 3780 (1995).

30. P. W. Dooley, I. V. Litvinyuk, K. F. Lee, D. M. Rayner, M. Spanner, D. M. Villeneuve, and P. B. Corkum, Phys. Rev. A **68**, 023406 (2003).

31. R. J. Levis, G. M. Menkir, and H. Rabitz, Science **292**, 709 (2001).

32. B. J. Sussman, D. Townsend, M. Yu. Ivanov, and A. Stolow, Science **314**, 278 (2006).

33. A. H. Zewail, J. Phys. Chem. A **104**, 5660 (2000).

34. J. P. Nibarger, M. Li, S. Menon, and G. N. Gibson, Phys. Rev. Lett. **83**, 4975 (1999).

35. L. Fang and G. N. Gibson, Phys. Rev. A **75**, 063410 (2007).

36. B. J. Pearson, S. R. Nichols, and T. Weinacht, J. Chem. Phys. **127**, 131101 (2007).

37. D. Geißler, B. J. Pearson, and T. Weinacht, J. Chem. Phys. **127**, 204305 (2007).

38. Z.-H. Loh, M. Khalil, R. E. Correa, R. Santra, C. Buth, and S. R. Leone, Phys. Rev. Lett. **98**, 143601 (2007).

39. Z.-H. Loh, C. H. Greene, and S. R. Leone, Chem. Phys., in press.

40. A. Rundquist, C. G. Durfee, III, Z. Chang, C. Herne, S. Backus, M. M. Murnane, and H. C. Kapteyn, Science **280**, 1412 (1998).

41. P. Andersen, T. Andersen, F. Folkmann, V. K. Ivanov, H. Kjeldsen, and J. B. West, J. Phys. B **34**, 2009 (2001).

42. D. L. Ederer and M. Manalis, J. Opt. Soc. Am. **65**, 634 (1975).

43. M. J. Frisch, G. W. Trucks, H. B. Schlegel et al., GAUSSIAN 98, Revision A.9, Gaussian, Inc., Pittsburgh PA, 1998.

44. A. D. Becke, J. Chem. Phys. **98**, 5648 (1993).

45. C. Lee, W. Yang, and R. G. Parr, Phys. Rev. B **37**, 785 (1988).

46. L. Andrews, F. T. Prochaska, and B. S. Ault, J. Am. Chem. Soc. **101**, 9 (1979).

47. A. W. Potts, H. J. Lempka, D. G. Streets, and W. C. Price, Phil. Trans. Roy. Soc. Lond. A **268**, 59 (1970).

48. J. Huang, D. Xu, W. H. Fink, and W. M. Jackson, J. Chem. Phys. **115**, 6012 (2001).

49. S.-Y. Chiang, Y.-S. Fang, K. Sankaran, and Y.-P. Lee, J. Chem. Phys. **120**, 3270 (2004).

50. M. Kawasaki, S. J. Lee, and R. Bersohn, J. Chem. Phys. **63**, 809 (1975).

51. J. B. Koffend and S. R. Leone, Chem. Phys. Lett. **81**, 136 (1981).

52. T. F. Hunter and K. S. Kristjansson, Chem. Phys. Lett. **90**, 35 (1982).

53. H. Xu, Y. Guo, S. Liu, X. Ma, D. Dai, and G. Sha, J. Chem. Phys. **117**, 5722 (2002).

54. G. A. Worth and L. S. Cederbaum, Annu. Rev. Phys. Chem. **55**, 127 (2004).

55. D. R. Yarkony, Rev. Mod. Phys. **68**, 985 (1996).

56. A. Cummings and G. O'Sullivan, Phys. Rev. A **54**, 323 (1996).

57. F. A. Parpia, C. Froese-Fischer, and I. P. Grant, Comput. Phys. Commun. **94**, 249 (1996).

58. L. Young, D. A. Arms, E. M. Dufresne, R. W. Dunford, D. L. Ederer, C. Höhr, E. P. Kanter, B. Krässig, E. C. Landahl, E. R. Peterson, J. Rudati, R. Santra, and S. H. Southworth, Phys. Rev. Lett. **97**, 083601 (2006).

59. R. J. van Brunt and R. N. Zare, J. Chem. Phys. **48**, 4304 (1968).

60. U. Fano and J. W. Cooper, Rev. Mod. Phys. **40**, 441 (1968).

61. J. Schirmer, M. Braunstein, M.-T. Lee, and V. McKoy, in *VUV and Soft X-Ray Photoionization*, edited by U. Becker and D. A. Shirley (Plenum Press, New York, 1996), pp. 105 – 133.

62. J. H. Johnson, J. N. Cutler, G. M. Bancroft, Y. F. Hu, and K. H. Tan, J. Phys. B **30**, 4899 (1997).

63. L. Andrews, J. M. Dyke, N. Jonathan, N. Keddar, and A. Morris, J. Phys. Chem. **88**, 1950 (1984).

64. L. V. Keldysh, Sov. Phys. JETP **20**, 1307 (1965).

65. M. V. Ammosov, N. D. Delone, and V. P. Krainov, Sov. Phys. JETP **64**, 1191 (1986).

66. A. M. Perelomov, V. S. Popov, and M. V. Terent'ev, Sov. Phys. JETP **23**, 924 (1966).

67. M. J. Rosker, M. Dantus, and A. H. Zewail, J. Chem. Phys. **89**, 6113 (1988).

68. M. Dantus, M. J. Rosker, and A. H. Zewail, J. Chem. Phys. **89**, 6128 (1988).

69. D. Zhong and A. H. Zewail, J. Phys. Chem. A **102**, 4031 (1998).

70. R. de Nalda, J. G. Izquierdo, J. Durá, and L. Bañares, J. Chem. Phys. **126**, 021101 (2007).

71. G. E. Busch and K. R. Wilson, J. Chem. Phys. **56**, 3638 (1972).

72. S.-C. Yang and R. Bersohn, J. Chem. Phys. **61**, 4400 (1974).

73. M. Dantus, M. J. Rosker, and A. H. Zewail, J. Chem. Phys. **87**, 2395 (1987).

74. R. B. Bernstein and A. H. Zewail, J. Chem. Phys. **90**, 829 (1989).

75. R. Kosloff, Annu. Rev. Phys. Chem. **45**, 145 (1994).

76. M. H. Beck, A. Jäckle, G. A. Worth, and H. –D. Meyer, Phys. Rep. **324**, 1 (2000).

77. T. Baer and W. L. Hase, *Unimolecular Reaction Dynamics: Theory and Experiment* (Oxford University Press, Oxford, 1996).

78. D. Mathur, Phys. Rep. **391**, 1 (2004).

79. I. V. Litvinyuk, K. F. Lee, P. W. Dooley, D. M. Rayner, D. M. Villeneuve, and P. B. Corkum, Phys. Rev. Lett. **90**, 233003 (2003).

80. D. Pinkham and R. R. Jones, Phys. Rev. A **72**, 023418 (2005).

81. D. Pavičić, K. F. Lee, D. M. Rayner, P. B. Corkum, and D. M. Villeneuve, Phys. Rev. Lett. **98**, 243001 (2007).

82. J. Muth-Böhm, A. Becker, and F. H. M. Faisal, Phys. Rev. Lett. **85**, 2280 (2000).

83. X. M. Tong, Z. X. Zhao, and C. D. Lin, Phys. Rev. A **66**, 033402 (2002).

84. G. M. Bancroft and J. S. Tse, Comment. Inorg. Chem. **5**, 89 (1986).

85. J. N. Cutler, G. M. Bancroft, and K. H. Tan, J. Chem. Phys. **97**, 7932 (1992).

86. T. K Kjeldsen, C. Z. Bisgaard, L. B. Madsen, and H. Stapelfeldt, Phys. Rev. A **68**, 063407 (2003).

87. G. E. Busch and K. R. Wilson, J. Chem. Phys. **56**, 3626 (1972).

88. H. B. Levene and J. J. Valentini, J. Chem. Phys. **87**, 2594 (1987).

TABLE I. Optimized geometric parameters for the $CH_2Br_2^{2+}$ dication ground state and the transition state en route to Coulomb explosion, as well as those for the CH_2Br^+ ground state. Due to the elongation of one of the C–Br bonds in the transition state, two sets of values for the CBr bond length and HCBr bond angle exist for that state.

	$CH_2Br_2^{2+}$ ground state	Transition state	CH_2Br^+ ground state
$r(CBr)$ / Å	1.999	1.773, 2.700	1.755
$r(CH)$ / Å	1.093	1.105	1.089
$\theta(BrCBr)$ / deg.	72.5	121.3	—
$\theta(HCH)$ / deg.	124.1	118.9	121.4
$\theta(HCBr)$ / deg.	112.2	118.9, 83.3	119.3

FIGURE CAPTIONS

FIG. 1. Schematic illustration of the experimental setup.

FIG. 2. Pump-probe time traces for (a) the growth of the $CH_2Br_2^+$ ion ground state and (b) the depletion of the neutral CH_2Br_2 molecule. These time traces give a Gaussian instrument response function with a FWHM of 37 fs.

FIG. 3. Energy level diagram showing the adiabatic correlation of the various $CH_2Br_2^+$ ion states to their respective dissociation products.

FIG. 4 (COLOR ONLINE). Soft x-ray transient absorption spectrum collected at a time delay of 500 fs and a moderate peak intensity of 2.0×10^{14} W/cm^2. The peaks at 64.4 eV, 65.1 eV, and 65.4 eV correspond to atomic Br transitions from the $3d$ core level, whereas the peaks at 66.5 eV and 67.3 eV correspond to transitions of parent $CH_2Br_2^+$ and fragment CH_2Br^+ in their electronic ground states. The shoulder at 66.0 eV corresponds to a transition from the $\widetilde{B}$ and/or $\widetilde{C}$ electronically excited state of $CH_2Br_2^+$. The solid line represents the fit of the entire spectrum to a sum of six Gaussian peaks, with each individual component appearing as a dotted line.

FIG. 5. Pump-probe time traces for the appearance of (a) the Br (●) and Br* (○) atoms, and (b) the CH_2Br^+ photofragment ion.

FIG. 6 (COLOR ONLINE). (a) Soft x-ray transient absorption spectrum collected at a time delay of 500 fs and a high peak intensity of 6.2×10^{14} W/cm^2. The peaks at 66.5 eV and 67.5 eV correspond to transitions of parent $CH_2Br_2^+$, whereas the peaks at 68.9 eV and 69.9 eV correspond to transitions of the $CH_2Br_2^{2+}$ dication. The depletion of neutral CH_2Br_2 appears at 70.5 eV and 71.6 eV. The solid line represents the fit of the entire spectrum to a sum of six Gaussian peaks (four of which have positive amplitudes and two have negative amplitudes), with each individual component appearing as a dotted line. The inset shows the absence of the atomic Br absorption peak at 64.4 eV. (b) Pump-probe time trace of the $CH_2Br_2^{2+}$ dication species.

FIG. 7. Energy level diagram for the Coulomb explosion of $CH_2Br_2^{2+}$, calculated at the B3LYP/6-311G(d,p) level of theory.

FIG. 8. Energy level diagram showing the effect of ligand-field splitting on the Br $3d^{-1}$ spin-orbit states, as well as the selective transition to the $^2\Sigma^+_{1/2}$ final core hole state from the $CH_2Br_2^+$ $\widetilde{X}$, $\widetilde{B}$, and $\widetilde{C}$ states by the soft x-ray probe pulse.

FIGURE 1

FIGURE 2

FIGURE 3

Energy (arb. unit)

$\widetilde{D}\ (^2B_2)$

$\widetilde{C}\ (^2A_1),$
$\widetilde{B}\ (^2B_1)$
$\widetilde{A}\ (^2A_2)$
$\widetilde{X}\ (^2B_2)$
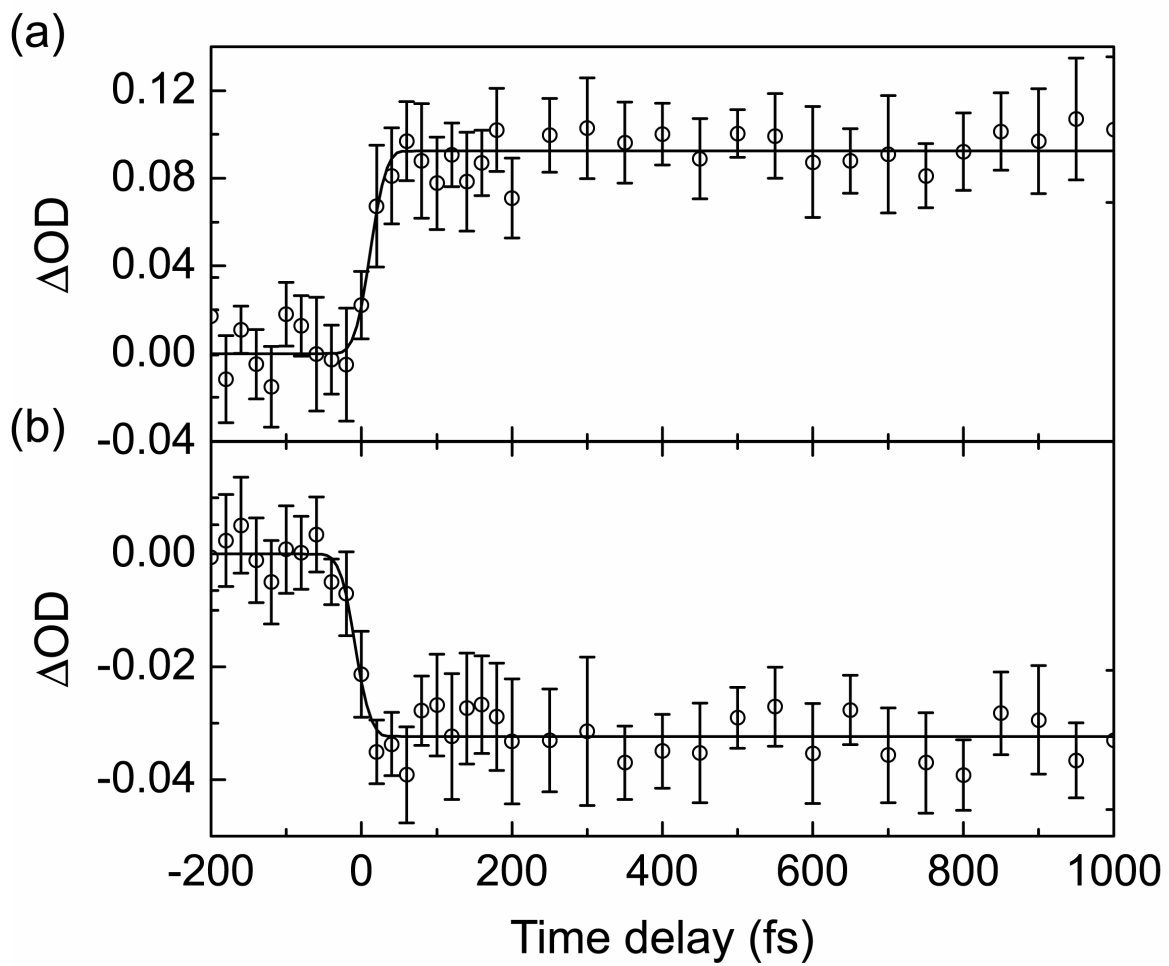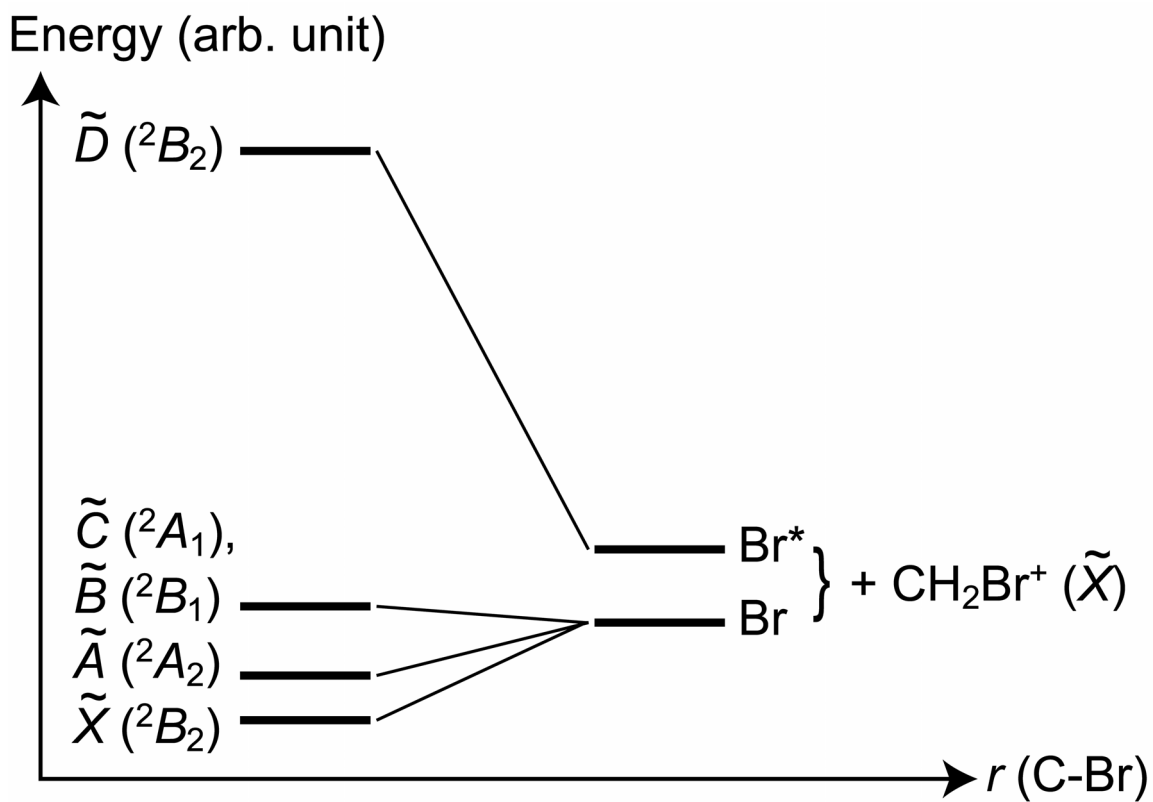
Br*
Br $\Bigg\}$ + CH_2Br^+ ($\widetilde{X}$)

r (C-Br)
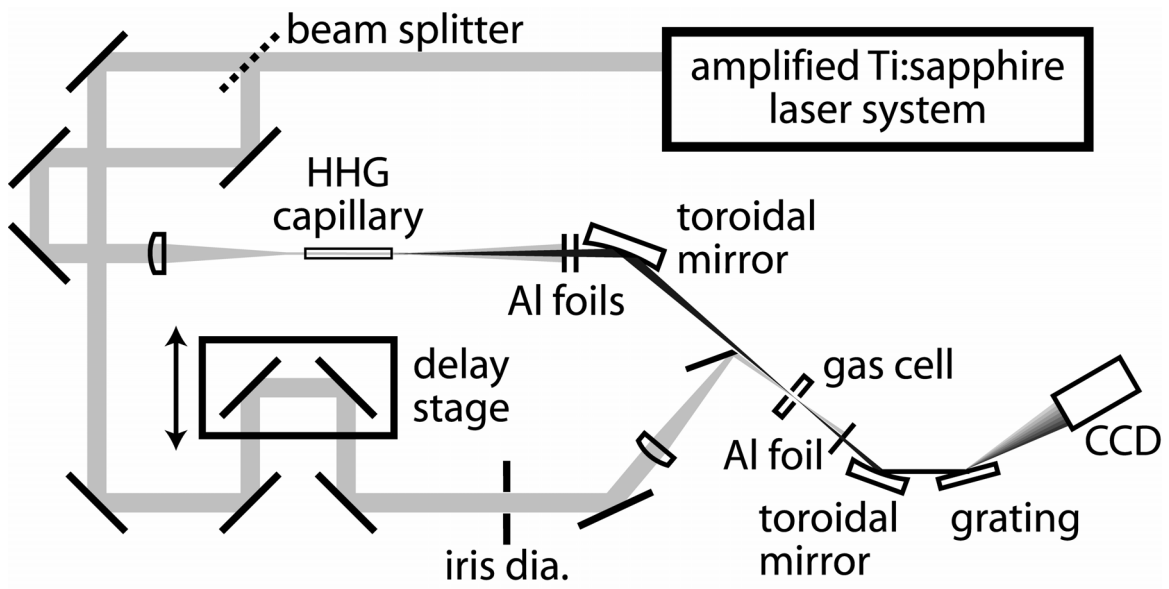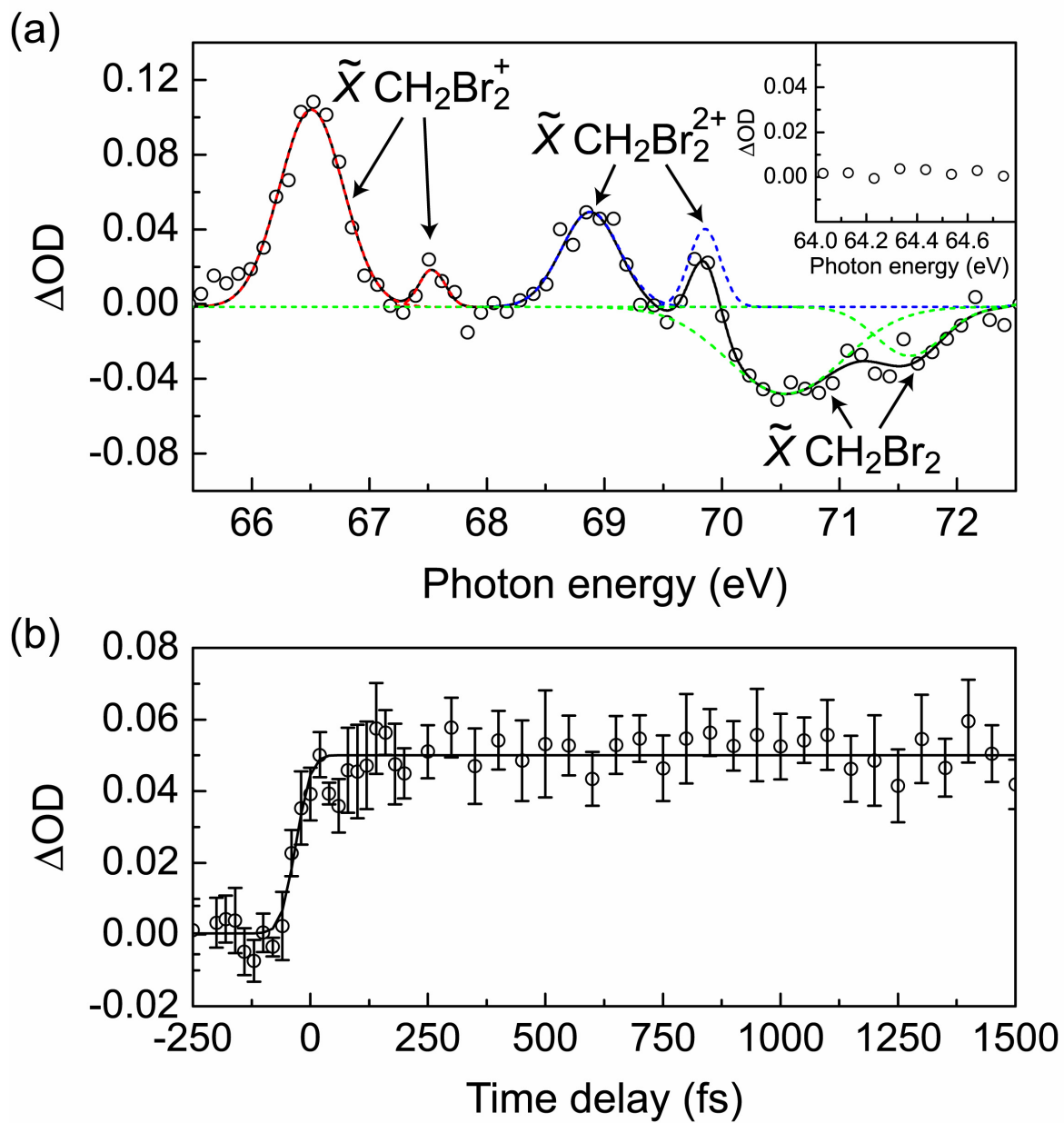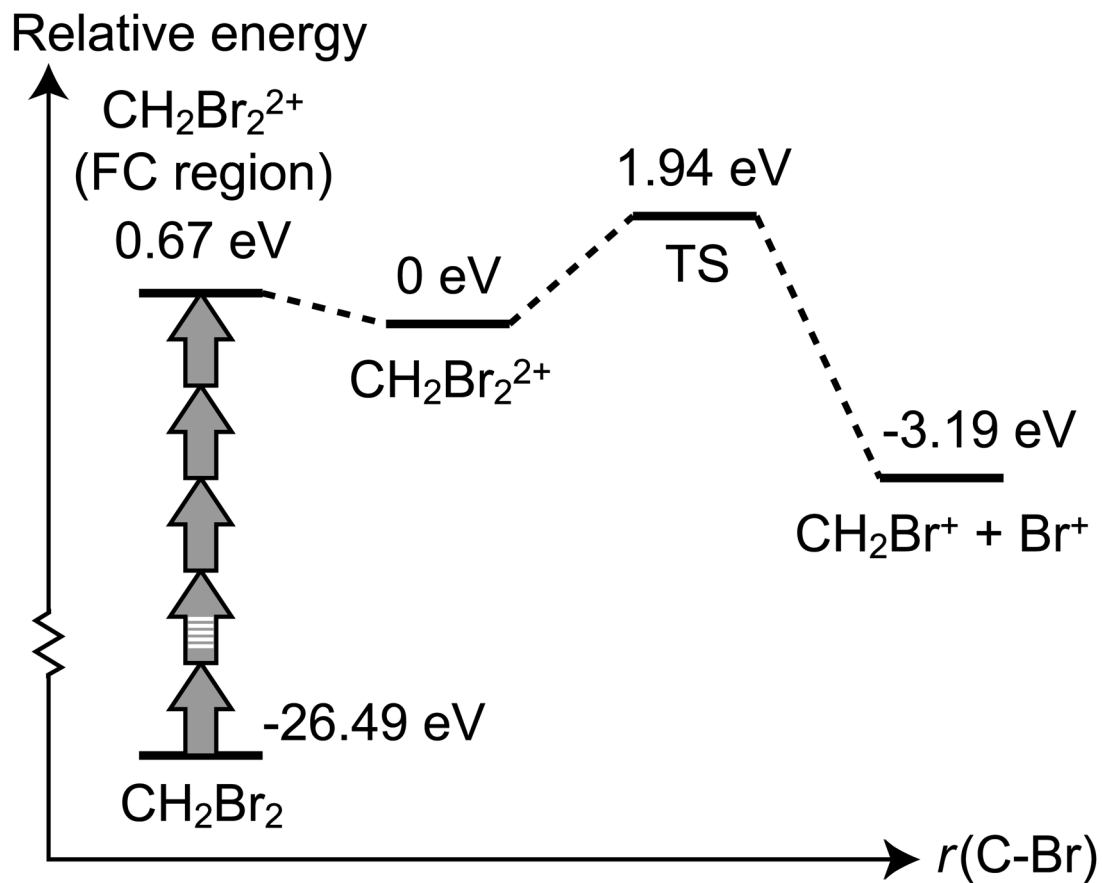
FIGURE 4 (COLOR ONLINE)
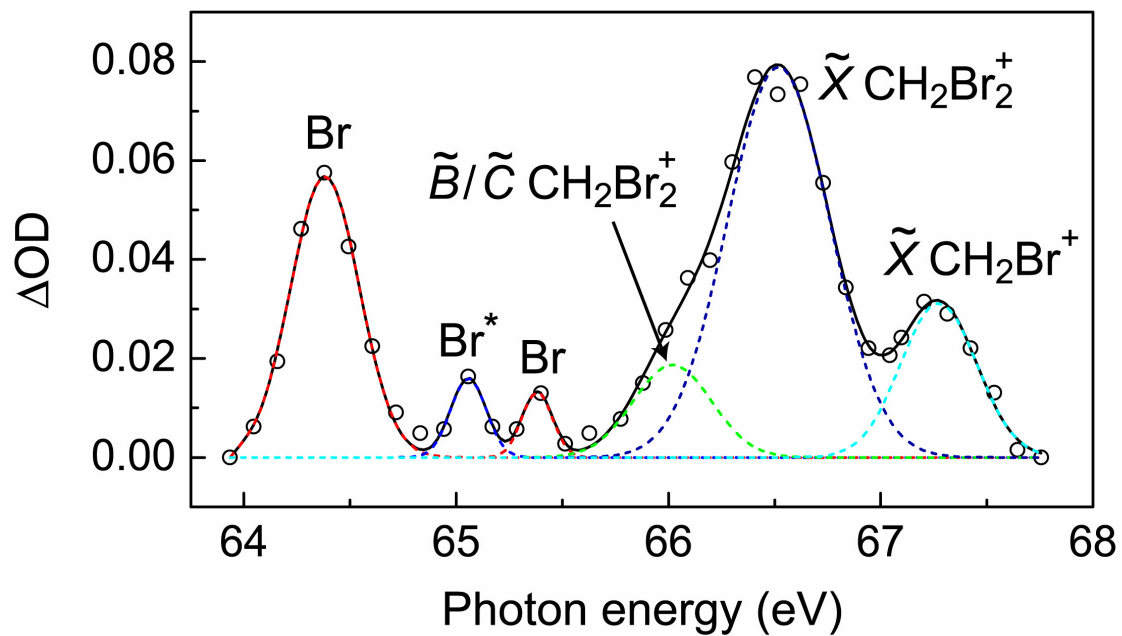
FIGURE 5

FIGURE 6 (COLOR ONLINE)

(a)

(b)

FIGURE 7

FIGURE 8